POLITECNICO
MILANO 1863

DIPARTIMENTO DI MECCANICA

mecc

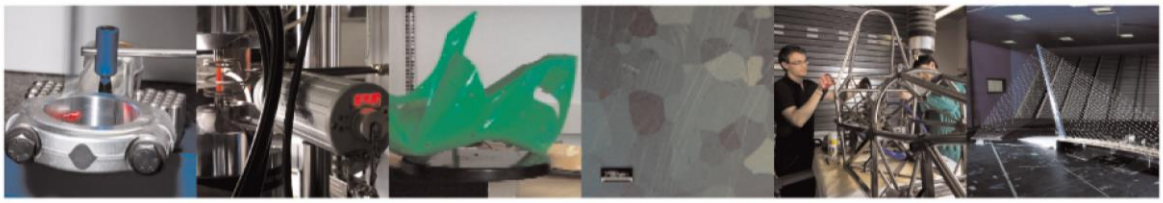

# Improvement of SLM Build Rate of A357 alloy by optimizing Fluence

S.Cacace, Q.Semeraro

This is a post-peer-review, pre-copyedit version of an article published in Journal of Manufacturing Processes. The final authenticated version is available online at: http://dx.doi.or10.1016/j.jmapro.2021.03.043



# Improvement of SLM Build Rate of A357 alloy by optimizing Fluence

Authors: S.Cacace[(a)*], Q.Semeraro[(a)]

[(a)]Dipartimento di Meccanica, Politecnico di Milano, Via La Masa 1, 20156 Milano

[*]stefania.cacace@polimi.it

## Abstract

Selective Laser Melting is one of the most widely used Additive manufacturing technologies for producing metal parts. Among the many advantages of SLM, the low build rate is still one of the most difficult challenges to address. The Build Rate (BR) of SLM depends on many factors, one of them is the scanning time which is directly related to Fluence. In this work, a procedure to select a process parameter combination with an increased BR is presented and validated experimentally. A357 alloy was selected to print tensile specimens using different combinations of process parameters resulting in the same value of Fluence, and four levels of Fluence are selected for the analysis. Despite the wide range of Fluence considered, 85 – 140 J/mm$^3$, the mechanical properties did not change. The combination of parameters ensuring the highest productivity was selected for the validation run. Experimental data were used to estimate regression equations able to predict the mechanical properties of the high-productivity condition. Density and UTS of the validation samples were accurately predicted by the regression equations, and they were consistent with the base material properties. The procedure allowed us to identify a combination of parameters ensuring an increase in productivity of 26% compared to the standard condition.

Keywords: Selective laser melting; regression; Fluence

## 1 Introduction

Selective Laser Melting (SLM) is an Additive Manufacturing technique allowing to produce 3D metal parts from CAD data. This technology has been widely used in the last 20 years to produce parts for several sectors, i.e. aerospace, automotive and biomedical above all. Despite the well-known advantages, many challenges are still to be faced to allow wider adoption of the technology [1]. First of all, SLM parts even if produced near-net-shape usually need expensive post-processing activities, such heat treatments to improve their mechanical properties [2] [3], or machining to improve geometrical accuracy and reduce surface roughness [4]. Most of the research on SLM has been focused on studying the influence of laser-related process parameters on the formation of porosity and the subsequent mechanical properties. These process parameters can be aggregated in the Fluence index (also called Energy Density), which is the amount of energy delivered by the laser per unit volume. For pulsed lasers, Volumetric Fluence $\left(\mathrm{J/mm^3}\right)$ is evaluated as [5]

$$F = \frac{P \cdot t}{d_p \cdot d_h \cdot z} \qquad (1)$$

Where P is the power (W), t is the exposure time (µs), $d_h$ is the hatch distance (µm), $d_p$ is the point distance (µm), and z is the layer thickness (µm). The Volumetric Fluence is defined for continuous lasers considering the laser speed, v; equal to the ratio between point distance and exposure time,

$v=d_p/t$ [6]. An absorptivity coefficient can be added to the numerator; however, absorptivity is considered constant for a given material, so it is not considered hereafter.

Many studies showed a clear relationship between part apparent density and Fluence for a wide set of different materials, Inconel 718 [7], stainless steel [8], Al [9], Ti64 [10] and Cu [11] to cite a few. This relationship is schematized in Figure 1. At low values of Fluence, the amount of energy delivered by the laser is not sufficient to completely melt the powders resulting in a type of defect called lack of fusion. At extremely high values of Fluence, other defects are formed. These defects are generated by irregular melt pool dynamics, causing the entrapment of gas in the solidified material, and these defects are referred to as keyhole porosity. The presence of a steady region, between a minimum and a maximum level of Fluence ($F_{min}$ and $F_{max}$ in Figure 1), indicates that there are several optimal processing conditions available for the processing of the material. A detailed state of the art on the relationship between Fluence and individual process parameters can be found in [12]. A previous study of the authors [12] using Maraging steel showed that in the steady region, i.e. where part density does not change with increasing Fluence, it is possible to choose different combinations of process parameters and the resulting static mechanical properties are not statistically different. This result implies that we could choose among different combinations of process parameters, and a smart selection could imply the use of a productivity objective function. A possible productivity objective function is the Build Rate $\left(\mathrm{cm}^3/\mathrm{h}\right)$, and in the case of SLM process it can be evaluated as:

$$BR = \frac{d_p \cdot d_h \cdot z}{t} = \frac{P}{F} \qquad (2)$$

This formula states that the Build Rate is directly proportional to the power and inversely proportional to Fluence. To increase BR with constant power, we need to reduce Fluence [13]. The relationship in eq. (2) is also valid for continuous lasers: in this case, the Build Rate is defined by the following equation $BR = v \cdot d_h \cdot z$, resulting in $BR = P/F$ as for pulsed lasers. Being the BR inversely proportional to Fluence, the selection of extremely productivity values leads to defects in the final part, as visible in Figure 1. For this reason, the choice of the optimal Build Rate is subjected to the constraint of avoiding the formation of lack of fusion porosity in the final part.

The formula in (2) is a proxy of the real build time. The total Build time in SLM can be described as the sum of two different components [14]. The first one concerns the fixed time needed during the process, such as recoating time, platform heating and platform lowering. The second component is the time needed to melt the cross-section of the part on each layer, and this component is described by equation (2). The first component depends on the machine used and the selected layer thickness for the process. Considering our problem, the first component is fixed. The second component is of our interest because it states that it is possible to increase the productivity of the SLM process by an appropriate selection of the process parameters. Other factors which can affect the build time are related to the complexity of the part to be produced: lattice structures and the presence of supports can lead to low production times, [15] [16].

Other authors studied how to improve the productivity of the SLM process. Sun et al. [17] increased power up to 380W to produce fully dense cubes in SLM using AISI 316L powders. They showed that high power levels allow increasing scan speed to obtain an increase in the build rate up to 70%. Spierings et al. in [18] proposed a different equation to estimate the build rate, which considers scanning time, layer thickness, downtime, and recoating time for the production of 17-4PH parts. Their results show that the scanning time is the most influential factor on the build rate. These results showed that the power of the laser should be kept at its maximum level if possible, to allow other

parameters to be optimized, and that scanning parameters have a strong impact on the BR of the SLM process. To obtain good mechanical properties when increasing the layer thickness, it is necessary to increase the power to guarantee the complete melting of the layer. As we are already working at the maximum power, the layer thickness was not modified in this experiment. In this work, we are providing a framework that allows comparing process parameters at different productivity levels without changing the geometry, orientation of the part and using a constant layer thickness.

The choice of the optimal process parameters considering the productivity maximization implies the minimization of Fluence, as clear from eq. (2), if power is kept constant. Fluence can be minimized until the full solidification of the material is achieved (Figure 1), to avoid lack of fusion defects that are considered the most detrimental ones for mechanical properties [19], [20]. The low build rates of SLM compared to other powder-bed fusion processes such as EBM, or worst with other traditional technologies is well known [21]. For this reason, it is of great industrial interest to increase the productivity of the process to reduce its cost and increase efficiency.

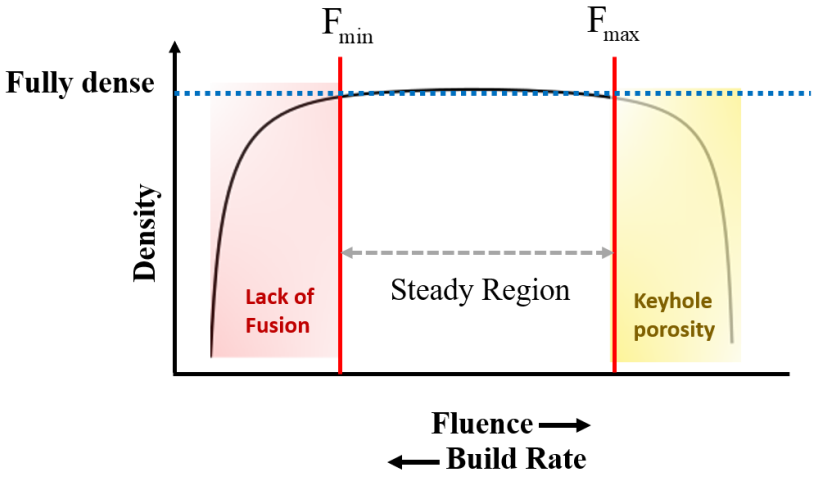


Figure 1 Porosity as function of Fluence and relationship with productivity

In this work we considered A357 alloy, which is a traditional cast Al-Si-Mg alloy which finds wide applications in the aerospace and automotive industries. It is characterized by good castability and weldability which make this material suitable for SLM process. A357 is characterized by good strength and high corrosion properties. However, A357 gained lower attention than others Al-Si-Mg alloys in SLM application, and the number of publications covering this alloy study is relatively small. Rao et al. in [22] studied the influence of process parameters (Power and scan speed) using an industrial system equipped with a laser working in continuous mode. The response analyzed in this work was the apparent density. The processing parameters optimized, ensuring the highest density, were then used to perform tensile tests at two different pre-heating temperatures. The effect of building pre-heating and post-process heat treatments on tensile properties was also studied in [23] using optimal process parameters. Heat treatments on tensile properties were also investigated in [24] and [25]. The fatigue behavior of A357 alloy was investigated in [26]. A summary of the tensile properties and optimal process parameters found in the literature for A357 is reported in Table 1.

Table 1. Summary of the state of the art on the tensile properties for A357 alloys processed via SLM process.

| Paper | F ($J/mm^3$) | Speed, mm/s | $d_h$, mm | Power, W | z, mm | Pre-heating | UTS (Mpa) | E % |
|---|---|---|---|---|---|---|---|---|
| [22] | 50 | 2000 | 0.1 | 300 | 0.03 | 35° | 395±4.7 | 5.1±0.4 |
| [22] | 61.6 | 2000 | 0.1 | 370 | 0.03 | 200°C | 290±2.9 | 3.2±0.3 |
| [23] | 41.7 | 1200 | 0.1 | 150 | 0.03 | 100° | 389±3 | 5.2±2 |
| [26] | 47.5 | 2000 | 0.2 | 950 | 0.05 | 200° | 305±15 | 3.5±0.7 |
| [24] | 108 | t=140 µs, $d_p$=80 µm | 0.115 | 200 | 0.025 | none | 398±13 | 10.1±0.5 |
| [27] | 54.2 | 1200 | 0.1 | 195 | 0.03 | 100° | 388±5 | 5.3±0.4 |

## 2 Objective of the work

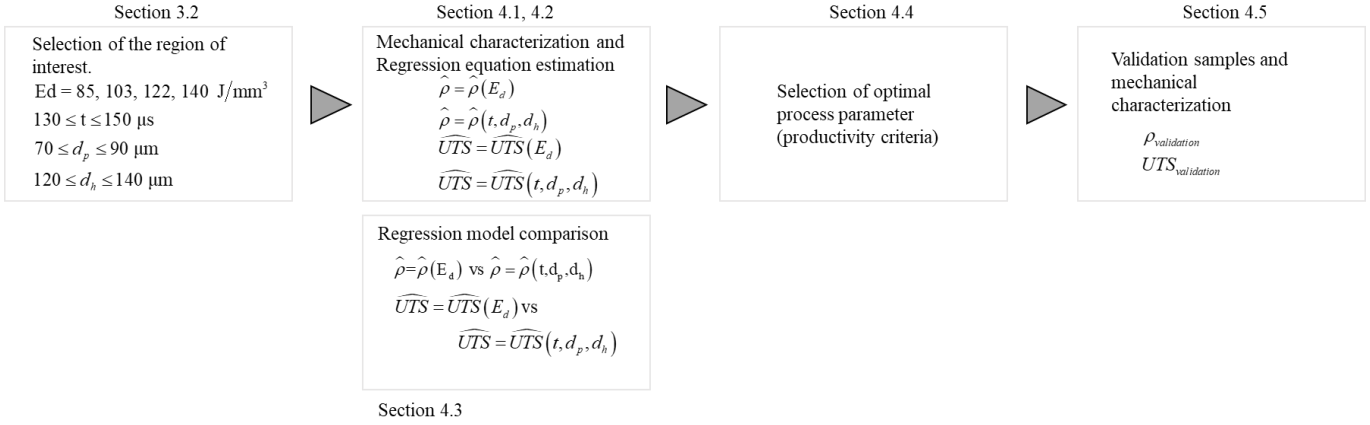


Figure 2. Workflow of the present work

In this work, we provide a framework to determine a high-productivity process parameter combination for the SLM process based on an experimental approach. From eq (2), we see that the maximization of BR implies the minimization of Fluence at constant power. However, eq (1) states that different combinations of process parameters can result in the same Fluence. To be able to maximize BR based on Fluence, we first need to test that a) mechanical properties do not depend on the individual process parameters b) Fluence can describe the mechanical properties of the part equally well as process parameters. Both these questions are addressed in the paper. If the mechanical properties depend on the individual process parameters, i.e. given the same Fluence the mechanical properties are not consistent, then to maximize BR we need to consider the individual parameters and not the aggregated index Fluence. On the contrary, if Fluence can be used in place of the individual parameters without losing information on the mechanical properties, the optimization of BR can be performed considering the minimization of Fluence. An appropriate experimental campaign was designed to study different combinations of process parameters resulting in the same Fluence. Based on the mechanical properties of the printed samples, regression models were used to study the relationship between Fluence and individual process parameters (Section 4.1 and 4.2). Confidence intervals built on the previously estimated regression models were used to compare their predictive properties (Section 4.3). In Section 4.4 we selected a new combination of process parameters based on the results obtained in the previous sections. The regression models estimated

previously were used to predict the mechanical properties (density and UTS) of the optimized combination, new samples were printed, and the mechanical properties were compared with the predicted values (Section 4.5). The workflow of the present work is presented in Figure 2.

# 3 Materials and methods

## 3.1 SLM machine and material

Renishaw AM 250 was used to produce all samples. The system is equipped with fiber laser working in pulsed mode. The maximum power is 200 W with a beam spot of approximately 70 µm at focal position. The working chamber is filled with inert gas to obtain an oxygen content lower than 1000 ppm. The scanning strategy employed is a meander scanning strategy with a rotation of 67° of the scanning lines at each layer. Two borders outline the 2D area of each section. A graphical representation of the scanning strategy is presented in Figure 2.

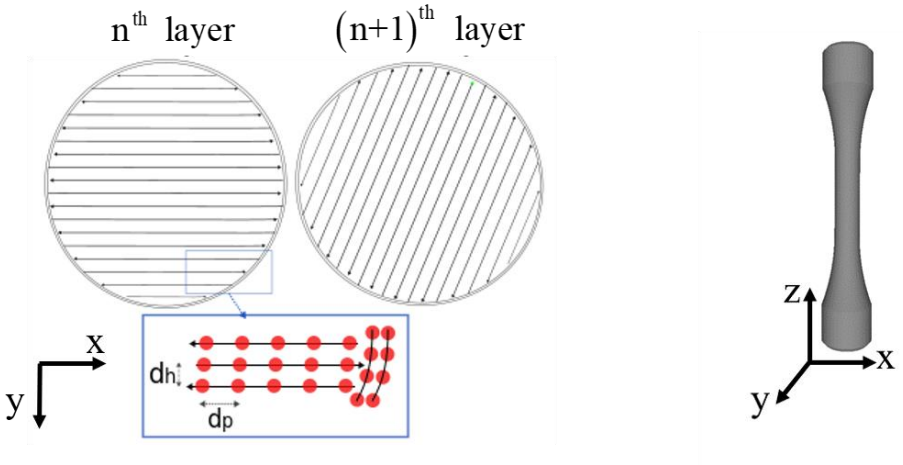


Figure 2. Graphical representation of point distance, hatch distance and scanning strategy and reference system for the tensile specimens.

A357 alloy was used for sample production. The metal powder was supplied by Carpenter Additive (Philadelphia, US). The powder granulometry follows a log-normal distribution with a mean Particle Size of 41.2 µm, while the morphology is shown in Figure 3. Powders showed a quasi-spherical shape with the extensive presence of satellites on the surface, which are a typical of the gas atomization process. The nominal chemical composition is presented in Table 2.

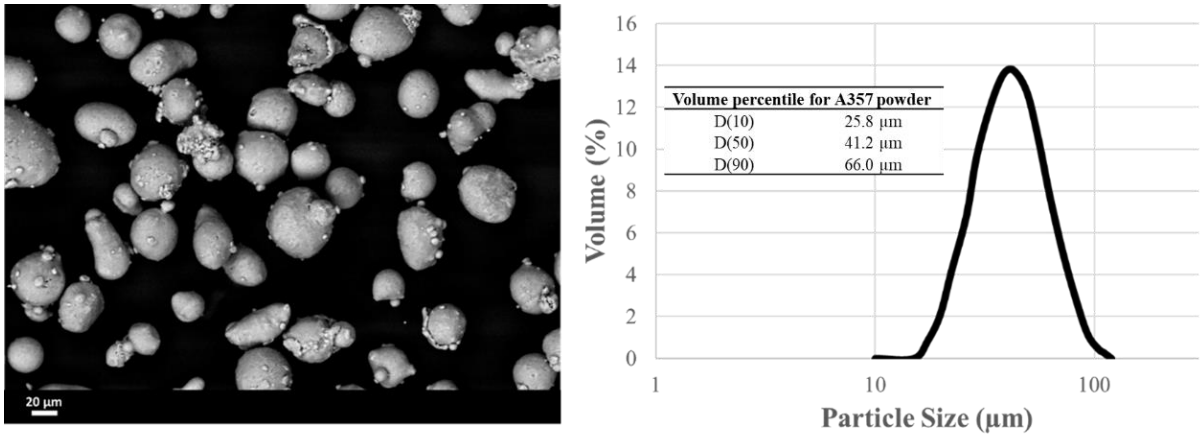


Figure 3. SEM image of A357 powders and particle size distribution.

Table 2. Nominal chemical composition of the investigated A357 powder (wt%)

| Al | Cu | Fe | Mg | Mn | N | O | Si | Ti | Zn |
|---|---|---|---|---|---|---|---|---|---|
| Bal | <0.05 | 0.1 | 0.58 | <0.1 | <0.2 | 0.1 | 6.5 | 0.12 | <0.1 |

### 3.2 Process parameters selection

The process parameters investigated in this study were exposure time, point distance and hatch distance. Table 2 shows the range of the varied parameter and, also the fixed experimental conditions. The range was selected starting from the recommended conditions by the machine manufacturer for A357, i.e. t = 140 µs, $d_p$=80 µm and $d_h$=130 µm. The intervals of the parameters were varied ±10% from the reference condition.

The layer thickness was set at 25 µm, while power was kept constant at its highest level (200 W).

Table 3. Process parameters investigated in the present experimentation.

| Varied parameters | | Fixed parameters | |
|---|---|---|---|
| Exposure time, t | 130 - 150 µs | Laser power | 200 W |
| Point distance, $d_p$ | 70 - 90 µm | Pre-heating | None |
| Hatch distance, $d_h$ | 120 – 140 µm | z | 25 µm |

Considering the above-stated ranges of the parameters, different combinations of (t, $d_p$, $d_h$) were generated resulting in specific values of Fluence, namely 85, 103, 122 and 140 J/mm$^3$. This range of Fluence is comparable with the levels selected in the literature (Table 1). The procedure used was described in a previous work by the authors [12]. The procedure works by selecting randomly a defined number of process parameters combination resulting in specific levels of Fluence, decided by the experimenter. A subset of these combinations was chosen by applying an optimization algorithm. As the input parameters of the machine are integer numbers, it was not possible to obtain combinations of these parameters that match exactly the desired level of Fluence. For this reason, a small deviation from the target was accepted ($\leq \pm 2$ J/mm$^3$). The procedure allowed obtaining Fluence values both lower and higher than the reference one. This choice is justified by two considerations. The reference condition might not be the optimal one from a productivity perspective, i.e. there might be other combinations of parameters resulting in a lower Fluence value and at least equally good mechanical properties. In addition, there might be a condition with higher Fluence than the reference condition resulting in higher mechanical properties. In this second case, the choice of the optimal condition depends on the specific application.

For each level of Fluence, three combinations of process parameters (t, $d_p$, $d_h$) were generated, resulting in 12 treatments (Table 4). Treatment 13 from Table 4 refers to the machine manufacturer suggested condition for A357 alloy. Then the minimum Fluence and maximum Fluence obtained using this limit were evaluated according to eq (1). The range of Fluence was then divided into four intervals. The percentage of variation of process parameters was selected to avoid a lower limit of Fluence which could not ensure a complete melting.

Table 4. Combinations of process parameters used in the study and reference condition.

| Treatment | t (µs) | dp (µm) | dh (µm) | F (J/mm$^3$) |
|---|---|---|---|---|
| 1 | 130 | 90 | 137 | |
| 2 | 132 | 90 | 139 | 85 |
| 3 | 131 | 88 | 139 | |
| 4 | 134 | 83 | 125 | |
| 5 | 135 | 87 | 120 | 103 |
| 6 | 148 | 83 | 137 | |
| 7 | 134 | 71 | 124 | |
| 8 | 137 | 74 | 121 | 122 |
| 9 | 141 | 70 | 131 | |
| 10 | 149 | 70 | 122 | |
| 11 | 149 | 71 | 120 | 140 |
| 12 | 148 | 70 | 120 | |
| 13 (reference) | 140 | 80 | 130 | 108 |

On each build, treatments 1-12 from Table 4 were replicated 3 times and treatment 13 was replicated 4 times, so the resulting number of samples is 40. Three identical builds were produced, so the total number of samples for the preliminary analysis was 40 samples x 3 builds = 120 samples.

The high number of replicates was needed to increase the accuracy of the analysis and it also allowed us to check the batch-to-batch variability of the process. The position of all samples was randomized in each build to avoid any effect of the position on the data analysis.

### 3.3 Mechanical characterization

Samples were characterized in terms of mean density and tensile properties. The relative density was measured by the Archimedes principle by weighting the sample in air and the in water. The final density is the mean of three measurement. The weights were measured using an electronic scale equipped with a kit for density measurement. Tensile samples were built without machining according to ASTM E8 standard. Tensile tests were performed with MTS Alliance RT100 machine according to the ISO 6892. Fracture surfaces and microstructural analysis were carried out using ZEISS Sigma 500 Scanning Electron Microscope. Samples were prepared by grinding and polishing and Keller's reagent was used to perform the microstructural analysis. The chemical composition was assessed by Optical Emission Spectroscopy OES (Bruker Q4 Tasman 130).

## 4 Experimental results

### 4.1 Density and tensile properties

Figure 4 shows the results of part density and UTS as function of Fluence and Treatment level. Regarding part density, all samples show a porosity lower than 1% despite the wide range of Fluence considered. The reference density considered for A357 is 2.68 g/cm$^3$ [22].

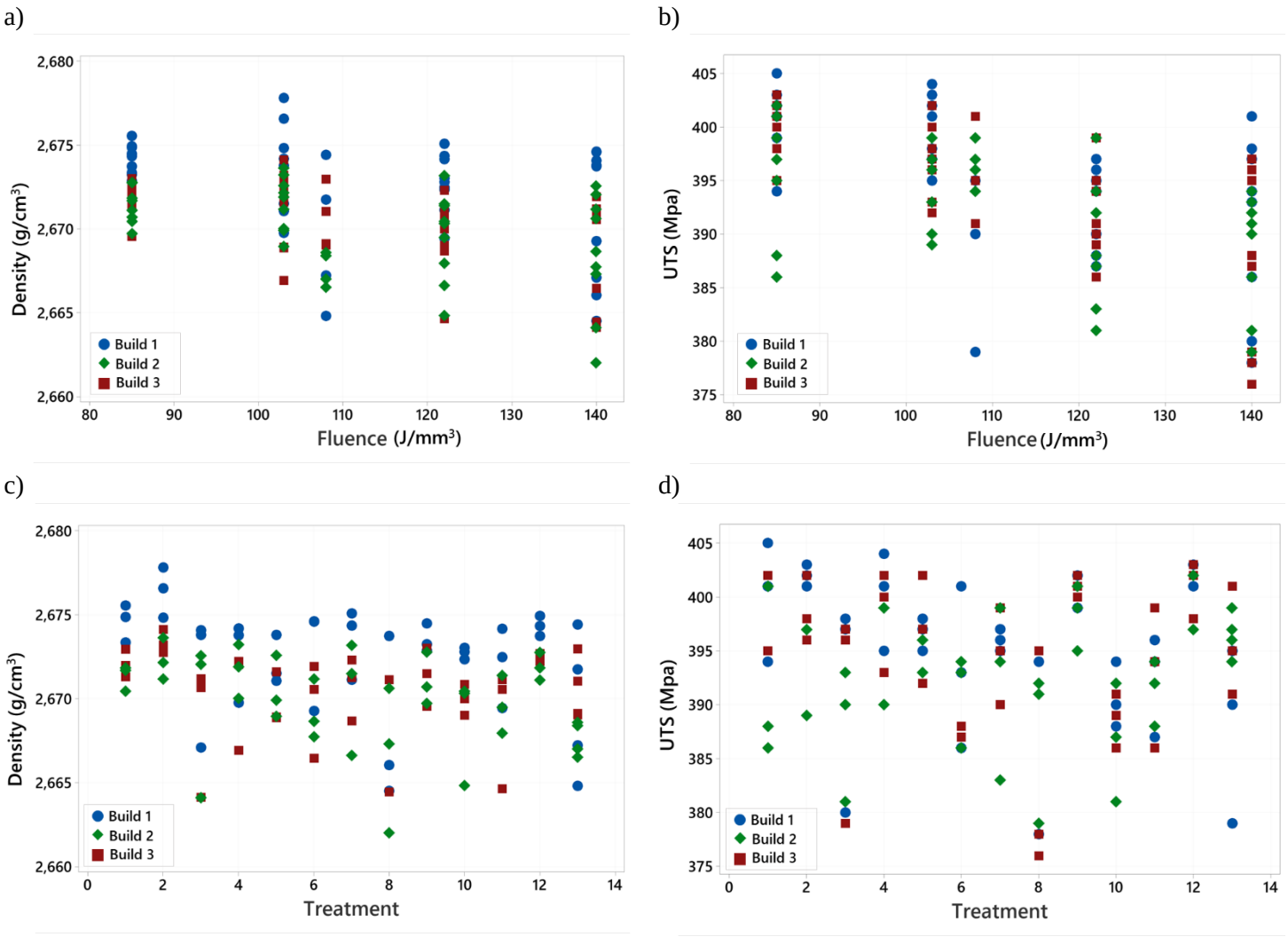


Figure 4 Part density a) and UTS b) plotted against Fluence and part density c) and UTS d) plotted for each Treatment level. Colours indicate different builds.

A slightly decreasing trend in density is visible as Fluence increases, however, the difference between the highest and least dense sample is lower than 7%. Ultimate Tensile Strength (UTS) is shown as reference for tensile properties, yield strength and elongation data are available in the Appendix. The range of UTS results is 30 MPa, meaning that in this range of Fluence and in this interval of parameters the mechanical properties of A357 alloy do not change from an engineering point of view. It is possible to identify a feasibility region where density and tensile properties do not change with process parameters. In terms of variability, density and UTS results show a moderate increase in the standard deviation with Fluence.

Table 5. Experimental tensile properties for A357 alloy.

| **Fluence** | **t, µs** | **$d_p$, µm** | **$d_h$, µm** | **P, W** | **Z, mm** | **Pre-heating** | **UTS (Mpa)** | **E, %** |
|---|---|---|---|---|---|---|---|---|
| 85-140 | 130 - 149 | 70 - 90 | 0.120 - 0.139 | 200 | 0.025 | none | 393±7.4 | 10.5±1.6 |

The summarized results of the present work in Table 5 can be compared with the literature data in Table 1. Authors who performed pre-heating during the process ([23], [26], [25]) obtained elongations values around 3-5%, while in this work and in [24] pre-heating was not applied and the resulting elongation is much higher.

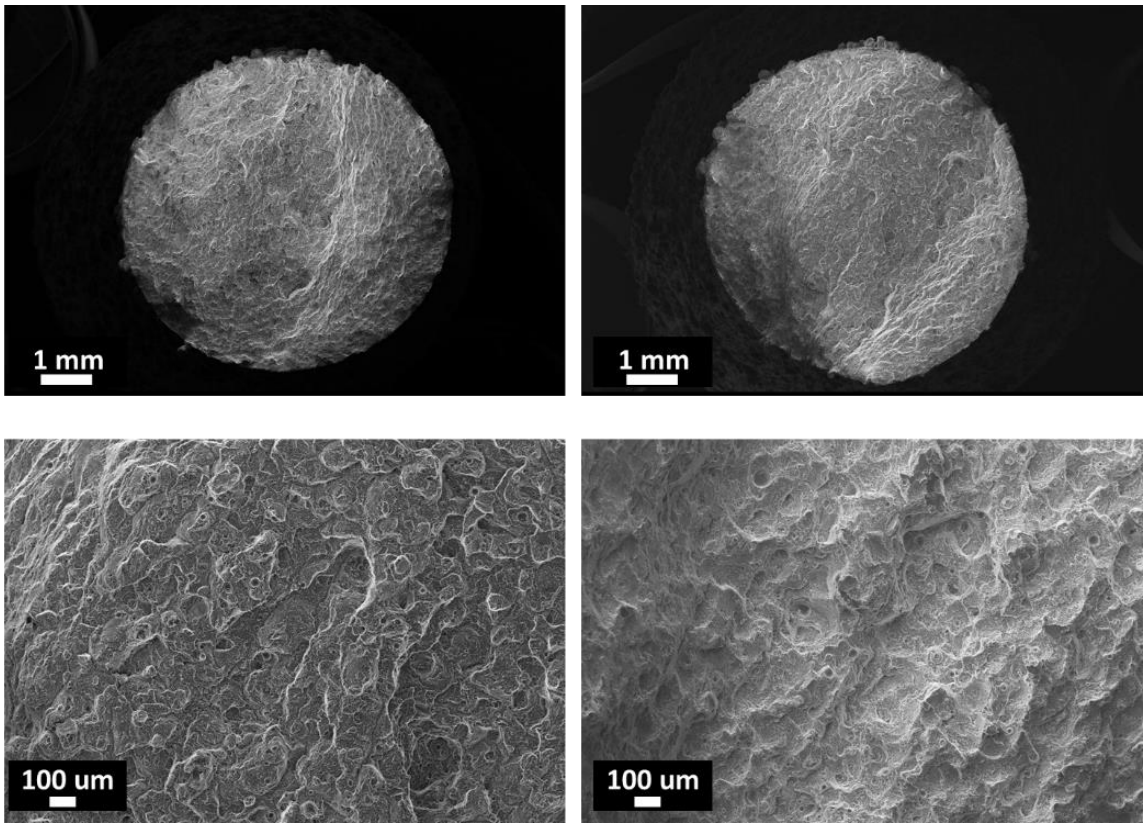


Figure 5 SEM Fractographic images of tensile sample a) produced with treatment 2, b) produced using manufacturer suggested process parameters.

There is a small difference in terms of tensile properties among the samples produced, so two fracture surfaces are analyzed with SEM. The detected breaks are classified as fragile breaks, and they do not present any relevant necking. Cleavage planes are visible in Figure 5. Similar fractographic images for as-built samples were showed by [25].
Summing up, the variation of the mechanical properties in the range 80-140 J/mm$^3$ is negligible: density is higher than 99% for all samples, while the range in UTS is 30 MPa.

The microstructure on the xy plane of reference samples at the different Fluence values was analyzed using an optical microscope and SEM. The optical micrographs (on the left in Figure 6) show identical features for all Fluence levels. The laser scans are visible with well-defined melt pool boundaries. The high-magnification of the surfaces of the samples (on the right in Figure 6) presents a cellular solidification structure typical of as-built Al-Si alloys processed by SLM. The extremely fine microstructure was detected in all samples, and it is due to the fast cooling during the process. The SEM images show fine Al grains surrounded by eutectic Si cells, as expected in this alloy [25]. Also, there is no evidence of differences in terms of microstructure among the levels of Fluence considered in this work regarding the cellular structure. A chemical analysis was performed on reference samples and the results are illustrated in Table 6; for each sample 4 replicated measurements were considered, and the average value is reported. The chemical analysis, as well as

the microstructural characterization, demonstrates that in the range of parameters and fluence considered there are no differences between the samples.

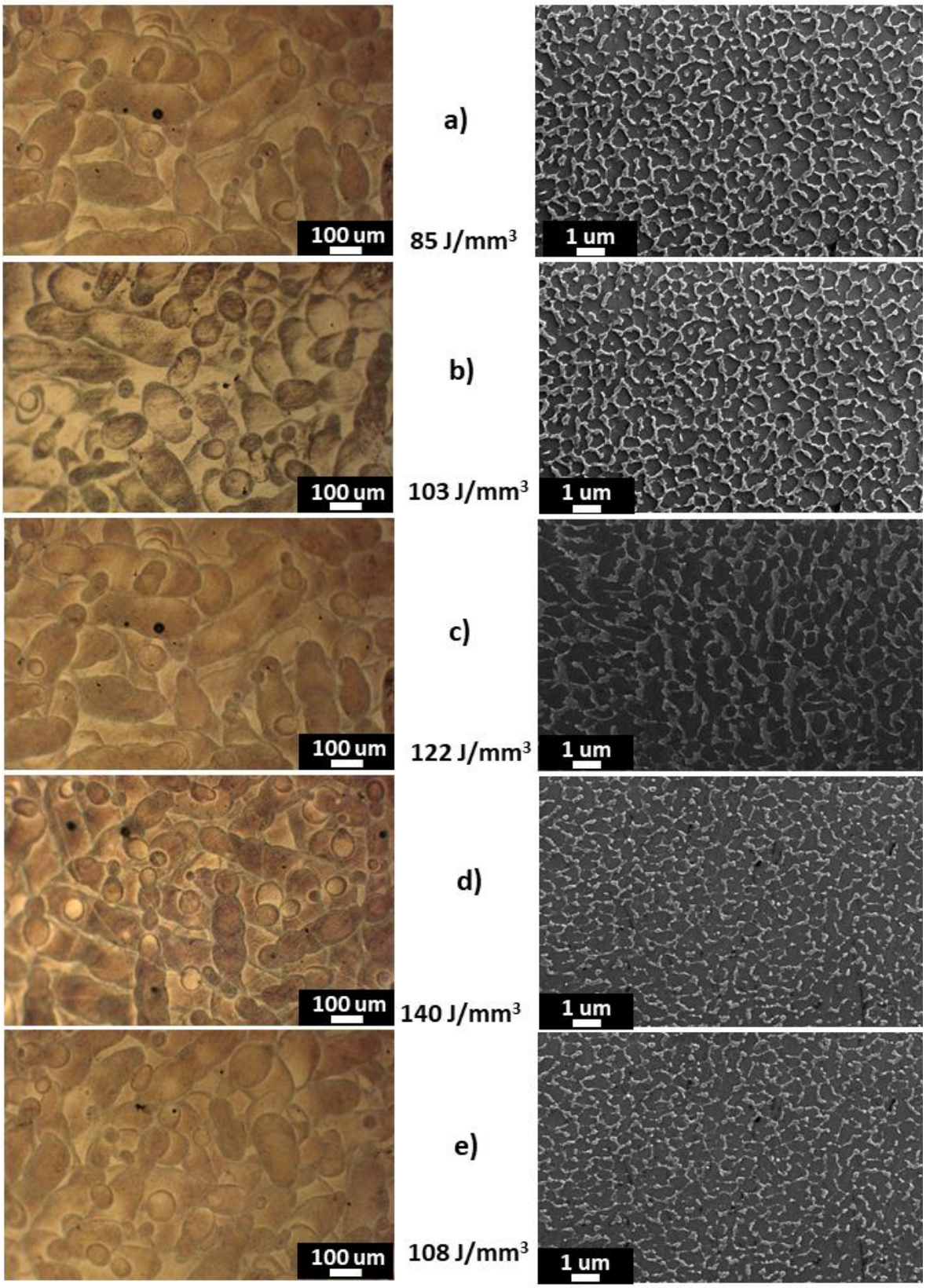


Figure 6. Optical and SEM high magnification images of the microstructure of the samples at different values of Fluence on the *xy* plane. a) F = 85 J/mm$^3$, b) F = 103 J/mm$^3$, c) F = 122 J/mm$^3$, d) F = 140 J/mm$^3$ and e) F = 108 J/mm$^3$ (reference condition).

| | Fluence [J/mm$^3$] | | | | |
|---|---|---|---|---|---|
| | **85** | **103** | **122** | **140** | **Reference condition** |
| Element | **Average** | **Average** | **Average** | **Average** | **Average** |
| Si | 6.269 | 6.277 | 6.352 | 6.258 | 6.353 |
| Fe | 0.050 | 0.057 | 0.047 | 0.042 | 0.044 |
| Cu | 0.0039 | 0.0042 | 0.0032 | 0.0032 | 0.0031 |
| Mn | 0.0014 | 0.0015 | 0.0014 | 0.0014 | 0.0014 |
| Mg | 0.657 | 0.682 | 0.647 | 0.630 | 0.613 |
| Zn | <0.0003 | <0.0003 | <0.0003 | <0.0003 | <0.0003 |
| Ti | 0.047 | 0.047 | 0.046 | 0.047 | 0.048 |
| Al | Balanced | Balanced | Balanced | Balanced | Balanced |

Table 6. Chemical composition (wt%) of A357 samples processed at different Fluence levels.

As mentioned in Section 3.2, the samples were produced in three non-consecutive builds and the influence of Fluence of the build for Density and UTS is shown in Figure 7.

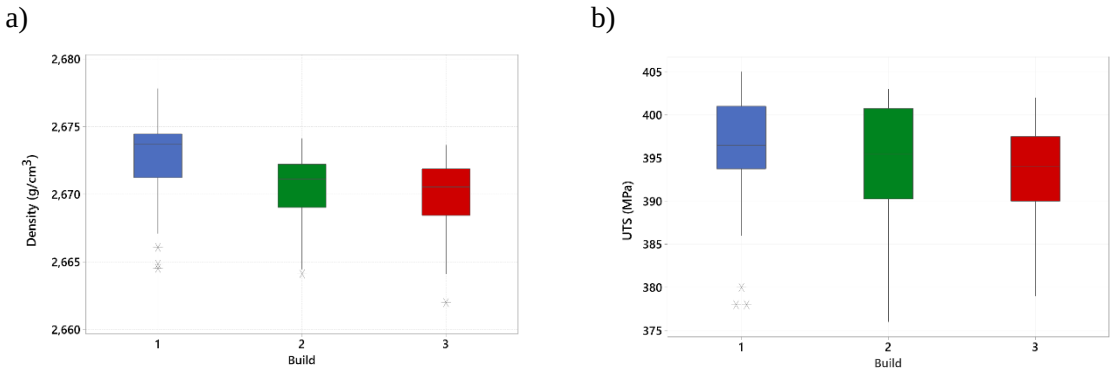


Figure 7. Batch-to-batch variability for a)density, b) UTS.

In terms of density, there is a slight decrease in density from build 1 (mean density 2.672 g/cm$^3$) to build 3 (mean density 2.670 g/cm$^3$). The difference is significant from a statistical point of view, but from an engineering perspective is minimal. UTS appears not to be influenced by the batch-to-batch variability, both in terms of mean value and standard deviation.

We conclude that in the process window considered in this study, all combinations of parameters used are equivalent from an engineering point of view and that the interval of fluence considered belongs to the steady interval shown in Figure 1.

## 4.2 Regression analysis

In this Section, regression analysis is used to prove if the mechanical properties of SLM parts can be described equally well using individual process parameters and Fluence. The regression equations are built considering both Fluence and individual process parameters. If the assumptions of the procedure are valid, these two models should result in the same quality of the prediction. The ANOVA table for the regression model of part density are showed in Table 7 and in Table 8.

Table 7 Regression Table for model $\rho_F = \rho_F\left(F\right)$

| Source | DF | Adj MS | F-Value | p-Value |
|---|---|---|---|---|
| Regression | 1 | 0.000105 | 14.65 | 0.000 |
| F | 1 | 0.000175 | 22.40 | 0.000 |
| Error | 117 | 0.000008 | | |
| Total | 118 | | | |

Table 8 Regression table for model $\rho_P = \rho_P\left(t, d_p, d_h\right)$

| Source | DF | Adj MS | F-Value | p-Value |
|---|---|---|---|---|
| Regression | 3 | 0.00062 | 8.46 | 0.000 |
| t | 1 | 0.00005 | 0.69 | 0.409 |
| $d_p$ | 1 | 0.000076 | 10.35 | 0.002 |
| $d_h$ | 1 | 0.000014 | 1.83 | 0.172 |
| Total | 118 | | | |

The regression equations are respectively:

$$\rho_F\left(F\right) = 2.677 - 0.000022 \cdot F \tag{3}$$

$$\rho_P\left(t, d_p, d_h\right) = 2.671 - 0.00004 \cdot t + 0.00017 \cdot d_p - 0.00006 \cdot d_h \tag{4}$$

Even though $d_h$ and t are not significant, they are included in the model to have all the components of the Fluence in the regression equation, as suggested by Montgomery [28] for regression analysis. The mean square errors of the two models are almost the same indicating that the two models are equally able to describe final part density despite using two different sets of parameters. Regression ANOVA tables for Ultimate Tensile Strength are reported in Table 9 and in Table 10.

Table 9 Regression table for model $UTS_F = UTS\left(F\right)$

| Source | DF | Adj MS | F-Value | p-Value |
|---|---|---|---|---|
| Regression | 1 | 1922.97 | 50.10 | 0.000 |
| F | 1 | 1922.97 | 50.10 | 0.000 |
| Error | 118 | 38.38 | | |
| Total | 119 | | | |

Table 10 Regression table for model $UTS_P = UTS\left(t, d_p, d_h\right)$

| Source | DF | Adj MS | F-Value | pValue |
|---|---|---|---|---|
| Regression | 3 | 685.14 | 18.08 | 0.000 |
| t | 1 | 24.676 | 0.65 | 0.421 |
| $d_p$ | 1 | 633.082 | 16.70 | 0.000 |
| $d_h$ | 1 | 0.645 | 0.02 | 0.896 |
| Error | 116 | 37.902 | | |

| | |
|---|---|
| Total | 119 |

The regression equations are respectively:

$$UTS_F\left(F\right) = 416.51 - 0.00806 \cdot F \quad (5)$$

$$UTS_P(t, d_p, d_h) = 369.9 - 0.088 \cdot t + 0.480 \cdot d_p + 0.013 \cdot d_h \quad (6)$$

Point distance is once again the main influencing factor for UTS, as it was for density. As for part density models, the mean square error of the UTS models based on Fluence and process parameters are similar.

### 4.3 Model comparison

The two fitted models are compared to verify if the models considering Fluence or individual process parameters predict the same mechanical values (density and UTS) and to check the prediction precision of the two models. To answer these two questions Confidence Intervals (CI) are used. First, models (3) and (4) are used to predict the mean density and confidence intervals in a new set of parameters $\left(t, d_p, d_h\right)$ resulting in the same value of Fluence. If the Confidence intervals based on models (3) and (4) overlap, it means that there is no difference in their prediction abilities. In addition, the width of the confidence intervals indicates how accurate is the prediction: a smaller width indicates a small uncertainty in the prediction. The width of the CI is evaluated as [28]:

$$\Delta_{IC} = 2 \cdot t_{\alpha/2}\left(df_E\right) \cdot \sqrt{\sigma \cdot \mathbf{x_0^T}\left(\mathbf{X^T X}\right)^{-1} \mathbf{x_0}} \quad (7)$$

Where $t_{\alpha/2}$ is the α/2-quantile of the t-student distribution with $df_E$ degrees of freedom, $df_E$ are the degrees of freedom of the error in the regression model, $\sigma$ is the estimated standard deviation of the regression model, $\mathbf{X}$ is the design matrix of the experiment and $\mathbf{x_0^T}$ is the point used for the prediction.

Let us start by analyzing density. Models $\rho_F\left(F\right)$ and $\rho_P\left(t, d_p, d_h\right)$ are used to evaluate CI estimates on three different values of Fluence, $F_i = \left[100, 112, 124\right]$ J/mm$^3$, with i=1,..,3. In the case of $\rho_F\left(F\right)$, only one CI can be generated for each value of Fluence $F_i$. In the case of model $\rho_P\left(t, d_p, d_h\right)$, for each level of $F_i$ one-hundred random combinations of $\left(t, d_p, d_h\right)$ are generated to calculate the CIs.

The result of the analysis for density is shown in Tables 9 and 10. The predicted value $\rho_F\left(F_i\right)$ and the width $\Delta_{IC,\rho_F(F_i)}$ of the CI for model $\rho_F\left(F\right)$ are reported, while for $\rho_P\left(t, d_p, d_h\right)$ the mean predicted value $\overline{\mathbb{E}}\left(\rho_P\left(t, d_p, d_h\right)\right)$ over the 100 CI's built and the mean width $\overline{\mathbb{E}}\left(\Delta_{IC,\rho_P\left(t,d_p,d_h\right)}\right)$ are shown in Table 11. The same procedure was followed also for UTS using models (5) and (6), and the results are reported in Table 12.

Table 11 Predicted density and width of CI's from models $\rho_F(F)$ and $\rho_P(t, d_p, d_h)$

| **Fluence (J/mm³)** | $\rho_F(F) \pm \Delta_{IC,\rho_F(F)}$ (g/cm³) | $\overline{\mathbb{E}}(\rho_P(t, d_p, d_h)) \pm \overline{\mathbb{E}}(\Delta_{IC,\rho_P(t,d_p,d_h)})$ (g/cm³) |
|---|---|---|
| 100 | 2.672 ± 0.0012 | 2.672 ± 0.0018 |
| 112 | 2.671 ± 0.0010 | 2.671 ± 0.0022 |
| 124 | 2.670 ± 0.0012 | 2.670 ± 0.0016 |

Table 12 Predicted density and width of CI's from models $UTS_F(F)$ and $UTS_P(t, d_p, d_h)$

| **Energy density (J/mm³)** | $UTS_F(F) \pm \Delta_{IC,UTS_F(F)}$ (MPa) | $\overline{\mathbb{E}}(UTS_P(t, d_p, d_h)) \pm \overline{\mathbb{E}}(\Delta_{IC,UTS_P(t,d_p,d_h)})$ (MPa) |
|---|---|---|
| 100 | 397 ± 2.10 | 397 ± 4.08 |
| 112 | 395 ± 1.50 | 394 ± 4.04 |
| 124 | 392 ± 2.08 | 391 ± 3.38 |

Looking at the results in Table 9 and Table 10, we can conclude that:

- The estimated expected values of the regression models are the same. From a practical point of view, it means that the properties of the prediction of the parts do not change when using Fluence or individual process parameters.
- The prediction precision is higher when Fluence is used as predictor, as shown by the width in Table 11 and Table 12.
- In the range of the parameters studied, the mechanical properties of A357 alloys do not change.

### 4.4 Selection of new process parameters

The results of the previous sections imply that we can optimize the BR of the process based on Fluence, i.e. using eq (2). Fluence will also provide a higher precision in the prediction of the properties of the validation samples. Since our objective is to choose the process parameter combination with the highest BR, we focus on the lowest value of Fluence, i.e. the highest productivity. Part density and UTS for highest productivity conditions (Treatments 1-3, F= 85 J/mm$^3$ and BR=8.57 cm$^3$/h) as well as reference condition (Treatment 13, F = 108 J/mm$^3$ and BR = 6.69 cm$^3$/h) are presented in Figure 8. The previous analysis results showed that the samples produced in the range of Fluence investigated are not different from a statistical point of view regarding apparent density and tensile properties. Additionally, the SEM images showed a similar microstructure at the different Fluence levels. One could choose any treatment at the highest build rate, which means selecting among Treatment 1, 2, and 3. The UTS variability at Treatment 3 was smaller than those obtained at Treatment 1 and 2, as visible in Figure 8. Even if this evidence is not supported with statistical significance (the p-value of the test for equal variances is larger than 0.05), Treatment 3 was selected for the validation step.

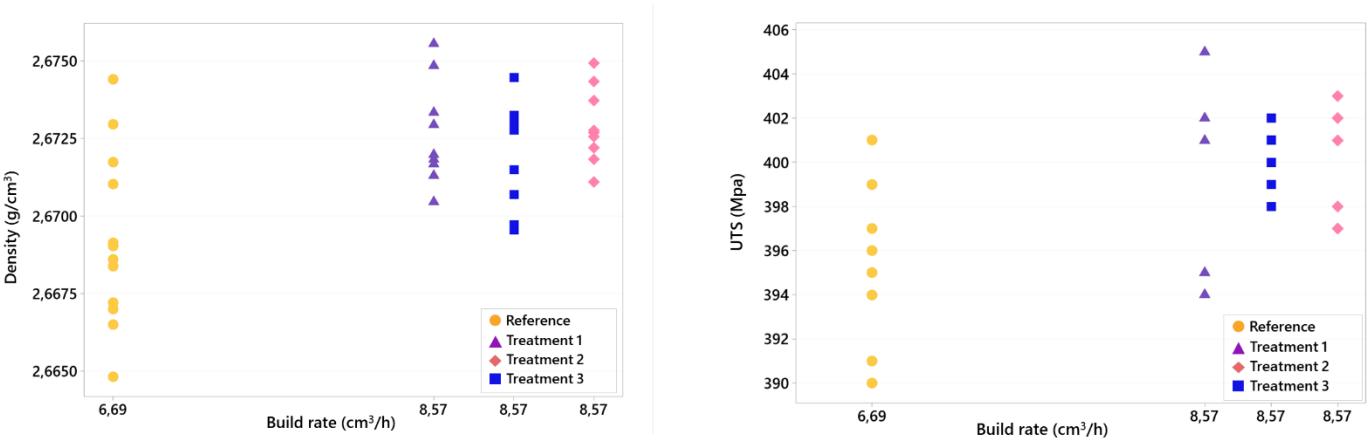


Figure 8 Part density a) and UTS b) as function of Build Rate. Data from Treatments 1-3 were jittered on the x-axis, but they all share the same BR.

### 4.5 Validation samples

The selected process parameters were used to produce five samples that were built using the same machine and powder, the validation samples are shown in Figure 9. Samples were characterized in terms of mean density and tensile properties. The results are used to validate the regression equations estimated in Section 4.2.

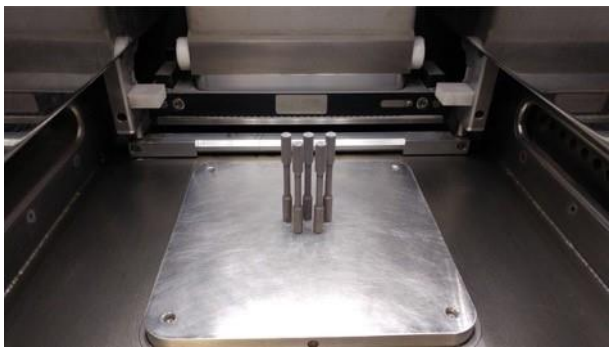

Figure 9. Validations samples

The prediction intervals (PI) based on equations (3-6) and the mechanical results of the validation samples are reported in Table 13. The mean density of the validation samples is 2.670 g/cm$^3$ (>99.5%) and the mean UTS is 412 MPa.

Table 13. Prediction interval for density and UTS based on model in equations (1-4) and results of the validation build

| Model | Prediction interval | Validation samples | |
|---|---|---|---|
| $\rho_F = \rho_F(F)$ | [2.672; 2.673] | 2.671<br>2.670 | g/cm$^3$ |
| $\rho_P = \rho_P(t, d_p, d_h)$ | [2.667; 2.678] | 2.672<br>2.672<br>2.671 | g/cm$^3$ |
| $UTS_F = UTS_F(F)$ | [397; 412] | 411<br>414 | MPa |

| | | |
|---|---|---|
| $UTS_P = UTS_P\left(t, d_p, d_h\right)$ | [386; 412] | 412<br>412<br>413 |

Models (3) and (4) predict similar final part density, the differences are in the range of the third decimal. This reflects the results showed in Section 4.1, where density did not vary in a significant way. Similar observations are obtained for UTS using models (5) and (6).

Once again, the result shows that the two sets of intervals overlap, which means that Fluence and individual process parameters predict the same mechanical property values. Moreover, the amplitude of the intervals based on Fluence is much smaller, as shown in Section 4.3. Density values of the validation samples belong to the PI of the Fluence, indicating that the smaller PI does not imply a lower accuracy.

UTS values of the validation samples belong to the prediction interval (except for one sample that exceeds the upper limit of 1 MPa). The improved mechanical properties could be attributed to the influence of the position of the validation samples. Models in equations (3) – (6) are estimated considering samples produced in a random position of the building platform, and it is known that position has influences the final part properties. The central position is favorable due to constant gas flow, while the lateral position might be influenced by turbulent flow [29]. It is likely that the validation samples resulting in higher mechanical properties due to their location at the center of the building platform (as visible in Figure 9).

In conclusion, by using the new set of parameters (Treatment 3) it was possible to produce samples with mechanical properties comparable with the reference value (Treatment 13) and a Build Rate of 8.54 $cm^3/h$.

Optimized and reference processing conditions are compared in Table 14. The last column of the table represents the improvement in Build Rate of the new processing condition for the validation runs compared to standard parameters (i.e. Treatment 13 in Table 4).

Table 14 Optimized process parameters for A357 alloy and productivity comparison with reference condition.

| **Treatment** | **t (µs)** | **dp (µm)** | **dh (µm)** | **F (J/mm³)** | **BR (cm³/h)** | **Improvement (%)** |
|---|---|---|---|---|---|---|
| 13 (Reference) | 140 | 80 | 130 | 108 | 6.7 | |
| 3 (Optimized) | 131 | 88 | 139 | 141 | 8.4 | +26% |

Optimized process parameters allow an improvement of 26% in terms of build rate without a negative impact on the mechanical properties. This improvement is even more important considering that Al alloys are usually processed using smaller layer thickness, hugely increasing the overall build time.

## 5 Conclusions

In this work, a procedure to select process parameters combination with an increased Build Rate is proposed. The procedure starts from the conjecture that Fluence and individual process parameters are equally able to describe the mechanical properties of the part, in a properly selected window of parameters. An experimental approach was used to test the procedure and validate this assumption.

Using an industrial SLM system, 120 samples were built in three batches using an Al alloy, A357. The range of Fluence considered varied from 85 to 140 J/mm3, i.e. BR from 5.15 to 8.46 $cm^3$/h.

We have experimentally proved that in the chosen range of process parameters, the mechanical properties (density and UTS), the microstructure and the chemical composition of the samples did not vary. Regression models were used to study how well Fluence, and individual process parameters were able to predict the mechanical properties of the parts. It was showed that Fluence and process parameters allowed to predict the same values of density and UTS, however Fluence resulted in higher precision.
Once that the assumption has been verified, the maximization of the BR implied the minimization of Fluence (power was kept constant for all the experiments). The combination of parameters that ensured the lowest variability at the lowest Fluence (85 J/mm3, 8.46 cm3/h) was selected for the validation test. Five validation samples were printed, and their mechanical properties were measured. All density values and UTS values were correctly predicted by the regression models using Fluence, despite the small width of the prediction intervals. The procedure allowed us to increase productivity by 26% compared to the standard parameter combination suggested by the machine manufacturer.

Future works will be focused on the study of the fatigue properties at fixed Fluence and the distribution, size, and shape of the porosity at different combinations of processing parameters in the steady region.

**Aknowledgments**

The Italian Ministry of Education, University and Research is acknowledged for the support provided through the Project "Department of Excellence LIS4.0 - Lightweight and Smart Structures for Industry 4.0".

**APPENDIX**

| | | UTS [Mpa] | | YS [Mpa] | | E [%] | |
|---|---|---|---|---|---|---|---|
| | | Mean | Std.dev | Mean | Std.dev | Mean | Std.dev |
| Fluence [J/$mm^3$] | 85 | 399,4 | 4,4 | 214,2 | 2,5 | 10,6 | 1,6 |
| | 103 | 397,4 | 4,1 | 210,8 | 2,7 | 10,9 | 1,6 |
| | 108 | 390,8 | 10,7 | 212,4 | 5,2 | 10,3 | 1,6 |
| | 122 | 391,7 | 4,9 | 206,9 | 4,4 | 10,4 | 1,3 |
| | 140 | 388,4 | 7,5 | 207,8 | 6,9 | 10,3 | 2,0 |

**BIBLIOGRAPHY**


[1] Tofail SAM, Koumoulos EP, Bandyopadhyay A, Bose S, O'Donoghue L, Charitidis C. Additive manufacturing: scientific and technological challenges, market uptake and opportunities. Mater Today 2018;21:22–37. https://doi.org/10.1016/j.mattod.2017.07.001.

[2] Prashanth KG, Scudino S, Klauss HJ, Surreddi KB, Löber L, Wang Z, et al. Microstructure and mechanical properties of Al-12Si produced by selective laser melting: Effect of heat treatment. Mater Sci Eng A 2014. https://doi.org/10.1016/j.msea.2013.10.023.

[3] Aboulkhair NT, Maskery I, Tuck C, Ashcroft I, Everitt NM. The microstructure and mechanical properties of selectively laser melted AlSi10Mg: the effect of a conventional T6-like heat treatment. Mater Sci Eng A 2016;104:174–82. https://doi.org/10.1016/j.msea.2016.04.092.

[4] Khorasani AM, Gibson I, Goldberg M, Littlefair G. A comprehensive study on surface quality in 5-axis milling of SLM Ti-6Al-4V spherical components. Int J Adv Manuf Technol 2018;94:3765–84. https://doi.org/10.1007/s00170-017-1048-9.

[5] Cherry JA, Davies HM, Mehmood S, Lavery NP, Brown SGR, Sienz J. Investigation into the effect of process parameters on microstructural and physical properties of 316L stainless steel parts by selective laser melting. Int J Adv Manuf Technol 2015;76:869–79. https://doi.org/10.1007/s00170-014-6297-2.

[6] Snow Z, Nassar AR, Reutzel EW. Invited Review Article: Review of the formation and impact of flaws in powder bed fusion additive manufacturing. Addit Manuf 2020;36:101457. https://doi.org/10.1016/j.addma.2020.101457.

[7] Jia Q, Gu D. Selective laser melting additive manufacturing of Inconel 718 superalloy parts: Densification, microstructure and properties. J Alloys Compd 2014;585:713–21. https://doi.org/10.1016/j.jallcom.2013.09.171.

[8] Haijun G, Rafi K, Karthik N V., Starr T, Stucker B. Influences of energy density on porosity and microstructure of selective laser melted 17-4PH. Proc Solid Free Fabr Symp 2013, Austin, TX 2013;474:12–4.

[9] Olakanmi EO. Selective laser sintering/melting (SLS/SLM) of pure Al, Al-Mg, and Al-Si powders: Effect of processing conditions and powder properties. J Mater Process Technol 2013;213:1387–405. https://doi.org/10.1016/j.jmatprotec.2013.03.009.

[10] Pal S, Lojen G, Kokol V, Drstvensek I. Evolution of metallurgical properties of Ti-6Al-4V alloy fabricated in different energy densities in the Selective Laser Melting technique. J Manuf Process 2018;35:538–46. https://doi.org/10.1016/j.jmapro.2018.09.012.

[11] Zhang G, Chen C, Wang X, Wang P, Zhang X, Gan X, et al. Additive manufacturing of fine-structured copper alloy by selective laser melting of pre-alloyed Cu-15Ni-8Sn powder. Int J Adv Manuf Technol 2018;96:4223–30. https://doi.org/10.1007/s00170-018-1891-3.

[12] Cacace S, Semeraro Q. About Fluence and Process Parameters on Maraging Steel Processed by Selective Laser Melting: Do They Convey the Same Information? Int J Precis Eng Manuf 2018;19:1873–84. https://doi.org/10.1007/s12541-018-0204-y.

[13] Matilainen V, Piili H, Salminen A, Syvänen T, Nyrhilä O. Characterization of process efficiency improvement in laser additive manufacturing. Phys Procedia 2014;56:317–26. https://doi.org/10.1016/j.phpro.2014.08.177.

[14] Schleifenbaum H, Meiners W, Wissenbach K, Hinke C. Individualized production by means of high power Selective Laser Melting. CIRP J Manuf Sci Technol 2010;2:161–9. https://doi.org/10.1016/j.cirpj.2010.03.005.

[15] Vaissier B, Pernot JP, Chougrani L, Véron P. Genetic-algorithm based framework for lattice support structure optimization in additive manufacturing. CAD Comput Aided Des 2019;110:11–23. https://doi.org/10.1016/j.cad.2018.12.007.

[16] Phatak AM, Pande SS. Optimum part orientation in Rapid Prototyping using genetic algorithm. J Manuf Syst 2012;31:395–402. https://doi.org/10.1016/j.jmsy.2012.07.001.

[17] Sun Z, Tan X, Tor SB, Yeong WY. Selective laser melting of stainless steel 316Lwith low porosity and high build rates. Mater Des 2016;104:197–204. https://doi.org/10.1016/j.matdes.2016.05.035.

[18] Spierings AB, Schoepf M, Kiesel R, Wegener K. Optimization of SLM productivity by aligning 17-4PH material properties on part requirements. Rapid Prototyp J 2014;20:444–8. https://doi.org/10.1108/RPJ-04-2013-0045.

[19] Yang K V, Rometsch P, Jarvis T, Rao J, Cao S, Davies C, et al. A Porosity formation mechanisms and fatigue response in Al-Si-Mg alloys made by selective laser melting. Mater Sci Eng A 2018;712:166–74. https://doi.org/10.1016/j.msea.2017.11.078.

[20] Krewerth D, Lippmann T, Weidner A, Biermann H. Influence of non-metallic inclusions on fatigue life in the very high cycle fatigue regime. Int J Fatigue 2016;84:40–52. https://doi.org/10.1016/j.ijfatigue.2015.11.001.

[21] Baumers M, Dickens P, Tuck C, Hague R. The cost of additive manufacturing: Machine productivity, economies of scale and technology-push. Technol Forecast Soc Change 2016;102:193–201. https://doi.org/10.1016/j.techfore.2015.02.015.

[22] Rao H, Giet S, Yang K, Wu X, Davies CHJ. The influence of processing parameters on aluminium alloy A357 manufactured by Selective Laser Melting. Mater Des 2016;109:334–46. https://doi.org/10.1016/j.matdes.2016.07.009.

[23] Aversa A, Lorusso M, Trevisan F, Ambrosio E, Calignano F, Manfredi D, et al. Effect of Process and Post-Process Conditions on the Mechanical Properties of an A357 Alloy Produced via Laser Powder Bed Fusion. Metals (Basel) 2017;7:68. https://doi.org/10.3390/met7020068.

[24] Casati R, Vedani M. Aging Response of an A357 Al Alloy Processed by Selective Laser Melting. Adv Eng Mater 2019;21. https://doi.org/10.1002/adem.201800406.

[25] Rao JH, Zhang Y, Fang X, Chen Y, Wu X, Davies CHJ. The origins for tensile properties of selective laser melted aluminium alloy A357. Addit Manuf 2017;17:113–22. https://doi.org/10.1016/j.addma.2017.08.007.

[26] Bassoli E, Denti L, Comin A, Sola A, Tognoli E. Fatigue Behavior of As-Built L-PBF A357.0 Parts. Metals (Basel) 2018;8:634. https://doi.org/10.3390/met8080634.

[27] Trevisan F, Calignano F, Lorusso M, Pakkanen J, Ambrosio EP, Mariangela L, et al. Effects of heat treatments on A357 alloy produced by selective laser melting. World PM 2016 Congr Exhib 2016:1–7.

[28] Montgomery DC. Design and Analysis of Experiments, 7th Edition. 2009.

[29] Ferrar B, Mullen L, Jones E, Stamp R, Sutcliffe CJ. Gas flow effects on selective laser melting (SLM) manufacturing performance. J Mater Process Technol 2012;212:355–64. https://doi.org/10.1016/j.jmatprotec.2011.09.020.